STUDIA UBB CHEMIA, LXVI, 3, 2021 (p. 63-72)
(RECOMMENDED CITATION)
DOI:10.24193/subbchem.2021.3.02

MAGNETIC AND TRANSPORT PROPERTIES OF DOUBLE PEROVSKITES

EMIL BURZO[a]

ABSTRACT. The magnetic and transport properties of polycrystalline Sr_2FeMoO_6 perovskites are strongly dependent on their microstructure. A cluster glass type behavior was shown at the grain boundaries. The increase of the sintering time from 4 to 8 hrs in $Sr_2FeMo_{1-x}W_xO_6$ and $Ca_{1.5}La_{0.5}FeMo_{1-x}W_xO_6$ series improves the crystallographic order. As a result there is an increase of both the saturation magnetizations and of spin polarizations.

Keywords: *perovskites, magnetic behavior, transport properties*

INTRODUCTION

The $A_2BB'O_6$ (A = Sr, Ca; B=Fe and B'=Mo) double perovskites are receiving attention due to their possible spin electronics applications and magnetoresistance based devices [1, 2]. The technical uses are facilitated by their Curie points located above ambient temperature.

The aristotype cubic ordered double perovskites A_2FeMoO_6 can be described by cubic sharing FeO_6 and MoO_6 octahedra, which alternate in three directions. The A site cations occupy the cavities formed by corner sharing octahedral network. Due to small Ca^{2+} cation radius, the FeO_6 and MoO_6 octahedra are considerably tilted in anti-phase order in the basal plane and along the crystallographic **c**-axis, the crystal structure of Ca_2FeMoO_6 decreasing, to monoclinic, space group $P2_1/n$ [3]. The crystal structure of Sr_2FeMoO_6, due to the same reasons, is tetragonal, space group I4/mmm [4].

The ideal magnetic structure of A_2FeMoO_6 can be described by an antiparallel arrangement of Fe^{3+} and Mo^{5+} magnetic moments, respectively [1]. The lower magnetization than the value of 4 μ_B/f.u., predicted by the above magnetic structure, is a general characteristic of these perovskites. This is the result of some competitive effects: (a) the presence of antisites, where the Mo atoms are located at the Fe position and vice versa; (2) the iron ions

[a] *Babeş-Bolyai University, Faculty of Physics, 1 Kogalniceanu str., RO-400028, Cluj-Napoca, Romania, emil.burzo@ubbcluj.ro*

having mixed valence states. In highly ordered Sr_2FeMoO_6, both Fe^{3+}-Mo^{5+} and Fe^{2+}-Mo^{6+} states are evidenced [5, 6]; (3) antiphase domains [7]; (4) nonuniform distribution of constituting elements inside and at the grain interface [8]; (5) oxidation at the grain boundaries; (6) decomposition of Sr_2FeMoO_6 sample with formation of $SrMoO_4$ [9], (7) changes with time of the Fe^{2+}/Fe^{3+} ratio [10] and (8) the Mo^{5+} moment smaller than 1 μ_B/ion.

The A_2FeMoO_6 double perovskites have half metallic behaviour under the assumption of a perfectly ordered crystal structure. In this case the down-spin conduction band crossing the Fermi level, E_F, is dominated by the Fe3d-Mo4d t_{2g} states, while the up-spin band, below E_F, is mostly due to the Fe3d e_g states [1]. Commonly, deviations from perfectly ordered crystallographic and magnetic structures are present, strongly influencing the transport properties.

Previously, we analysed the magnetic and transport properties of $Sr_2FeMo_{1-x}M_xO_6$ with M = W, Ta [11, 12], $Ca_{1.5}La_{0.5}FeMo_{1-x}W_xO_6$ [13] and $A_2Fe_{1-x}Ni_xMoO_6$ with A = Ca [14, 15] and Sr [16]. Some of these perovskites have Curie temperatures above the ambient one and thus possible technical uses. The physical properties were shown to be influenced both by composition and the sintering process. As an ongoing work on double perovskites, the effects of thermal treatment and sample compositions on the magnetic and transport properties of Sr- and Ca-based double perovskites are investigated.

RESULTS AND DATA ANALYSIS

The Sr_2FeMoO_6 perovskites were sintered at 1300 ^oC under argon flow with 1.7 % (sample S-3) and 0.8 % (sample S-5) hydrogen, at T = 1300 ^oC. The determined AS content by XRD was 3 % for sample S-3 and 5 % for the perovskite S-5. The XPS studies indicate the presence of 70 % Fe^{3+} - Mo^{5+} and 30 % Fe^{2+}-Mo^{6+} states.

The microstructure of sample S-3 consists from grains having 0.2-0.3 μm diameter and also regions in which the grain coalesced in bands, while the perovskite S-5 is constituted from grains having 2-3 μm dimensions. The iron content in sample S-3 was little smaller, while in perovskite S-5 higher than the ideal value (25 %). The molybdenum content decreased little from the center of the grain towards their boundaries. Around the grain boundaries the iron content was by 0.7 % (S-3) and 1.5% (S-5) higher than that inside the grains.

The analysis of the ^{57}Fe Mössbauer spectra, for the two Sr_2FeMoO_6 perovskites showed: (1) the AS content was 3.9 % in sample S-3 and 6.5 % in perovskite S-5, in rather good agreement with the values obtained from XRD method; (2) an iron-fraction of 5.8 % in S-3 and 6.2 % in S-5

perovskites, respectively are located in the antiphase domain boundaries (APB). The above differences in the microstructures of the two Sr_2FeMoO_6 perovskites are reflected in their magnetic and transport properties.

The temperature dependence of magnetization for sample S-3 is given in Fig.1.The saturation magnetization at 4.2 K, M_s=3.4 μ_B/f.u., is by 0.6 μ_B smaller than that estimated assuming a ferrimagnetic ordering and the already determined antisite fractions and iron valence states. The molybdenum moment was assumed to be $\cong$ 0.4 μ_B/atom, as determined by neutron diffraction study [17]. These data suggest the presence of antiphase domains and possible cluster glass type ordering at the grain boundaries. The saturation magnetization of sample S-5 is by $\cong$ 0.1 μ_B smaller than that of S-3 one, correlated with a larger fraction of antisites and APB. The saturation magnetization of sample S-3 decreased by 0.15 μ_B/f.u. by keeping in air around 9 months.

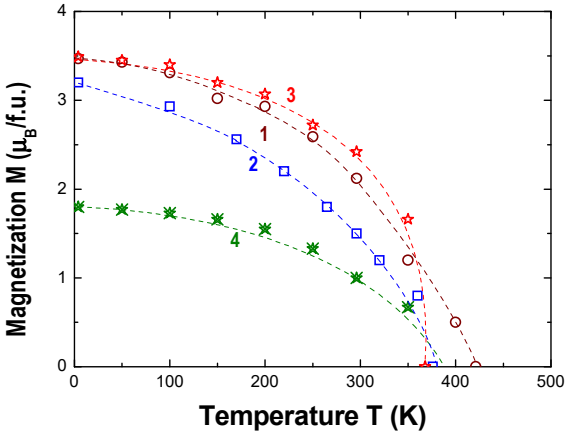

Figure 1. Thermal variations of magnetizations in 1-Sr_2FeMoO_6 (S3), 2-$Sr_2FeMo_{0.7}W_{0.3}O_6$, 3-$Ca_{1.5}La_{0.5}FeMoO_6$ and 4-Ca_2FeMoO_6 double perovskites

The magnetization isotherms, M(H), at T=4.2 K, do not follow the classical approach to saturation law, suggesting the presence of an additional small magnetic contribution superposed on that due to ferrimagnetic-type ordering. The better agreement with experimental data was obtained when the M(H) curves were analyzed assuming a field dependence, typical for a cluster glass system with weak anisotropy [18] – Fig.2.

$$m(H) = M(H)/M_s = (1-aH^{-1/2}) \quad (1)$$

By fitting the magnetization isotherms at T=4.2K, with the relation (1), values a = 0.15$T^{1/2}$ for sample S-3 and 0.18 $T^{1/2}$ for the perovskite S-5, respectively were obtained. The above results show the presence of cluster glass type behavior at the grain boundaries, which is superposed on the main magnetic contribution resulting from the antiparallel alignment of B(Fe) and B'(Mo) magnetizations.

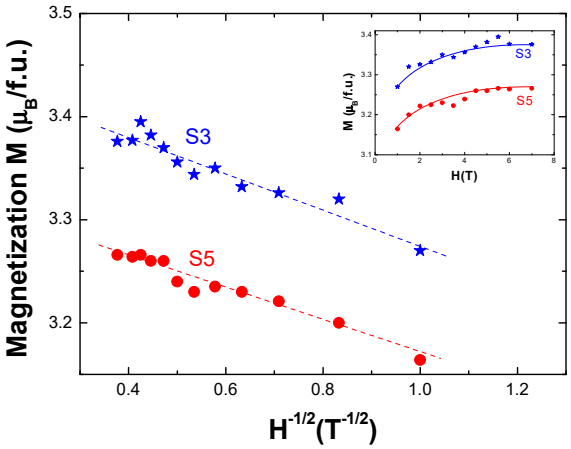

Figure 2. The magnetization isotherms, at T = 4.2 K, for two Sr_2FeMoO_6 perovskites (inset) and the dependences of the magnetizations, at T = 4.2 K on $H^{-1/2}$. The fitted curves are shown by dashed lines.

The previous studies on Sr_2FeMoO_6 perovskites showed both semiconducting and metallic behavior, depending on the preparation method [19, 20]. Differences between resistivities of the two Sr_2FeMoO_6 samples correlated with their microstructures, are also present, as seen in Fig.3. The perovskite S-3 has a resistivity by two orders of magnitude lower than that of the S-5 sample. The higher resistivity of sample S-5 can be attributed mainly to differences in the compositions inside the grains and at their interfaces. The iron content at the grain boundary is by ≅ 1.5 % higher, and consequently the cluster glass contribution to the magnetizations, as suggested from the analysis of magnetizations isotherms. The number of antisites in sample S-5 is twice than that in perovskite S-3. The lower hydrogen content in the mixture with argon, used during sintering, can lead to possible oxidation of the grain boundaries, affecting also the transport properties of sample S-5.

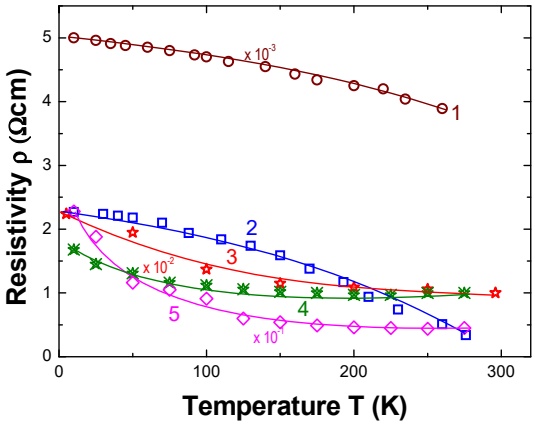

Figure 3. The temperature dependences of the resitivities for 1-Sr_2FeMoO_6 (S-3), 2 – Sr_2FeMoO_6 (S-5), 3-$Sr_2FeMo_{0.7}W_{0.3}O_6$-8hrs, 4-$Ca_{1.5}La_{0.5}FeMoO_6$ and 5-$Ca_{1.5}La_{0.5}FeMo_{0.7}W_{0.3}O_6$

The magnetoresistances (MR) of the perovskites are determined by two contributions: (1) the spin disorder inside the grains, proportional to the external field, $MR_d = -bH$; (2) the intergrain magnetic tunneling magnetoresistance (ITMR) which depends of the structure and magnetic state at the grain boundaries. The contribution of magnetic state at the grain boundaries to the ITMR, MR_i, in polycrystalline perovskites, can be analysed for systems where the applied field is smaller than the exchange field [21, 22]. By using the mean field approximation, the exchange interactions parameters inside and between the B and B' magnetic sublattices in Sr_2FeMoO_6, were determined ($J_{BB'} = -17$, $J_{BB} = 98$) and on this basis, the exchange field. The exchange field acting on B sublattice, of 200 T, is by ≅ 30 times higher than the field used in present measurements. Consequently, the model [21, 22] can be used also in analysing the transport properties of A_2FeMoO_6-based series.

Starting from a network of tunnel junctions, whose electrodes are double perovskite grains, separated by an insulating layer and assuming elastic tunneling across a single barrier, averaged over random grain orientations, the MR_i contribution to magnetoresistance can be described by [22]:

$$MR_i = \Delta\rho(\Delta H,T)/\rho(H,T) = -P^2m(H)^2[1+P^2m(H)^2]^{-1} \quad (2)$$

By P is denoted the spin polarization and m(H) is the reduced magnetization at the grain boundaries, given by the relation (1). As seen from Fig. 4, the low field magnetoresistance of polycrystalline perovskites is determined by spin polarized tunneling between the grains and the high field contribution is related mainly to the intragrain contribution.

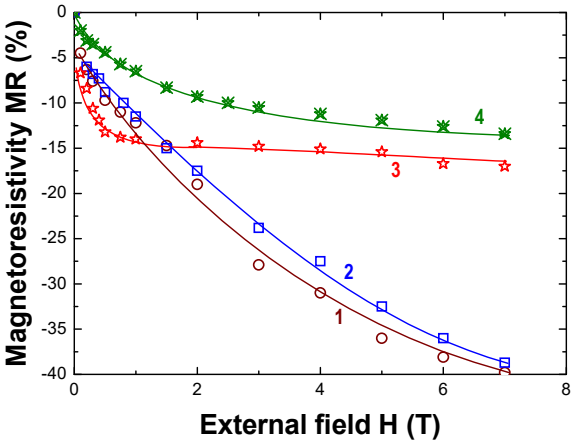

Figure 4. The field dependences of the magnetoresistances, at T = 10 K for 1-Sr_2FeMoO_6 (S-3), 2-$Sr_2FeMo_{0.7}W_{0.3}O_6$, 3- Ca_2FeMoO_6 and 4-$Ca_{1.5}La_{0.5}FeMoO_6$

By fitting the experimentally determined magnetoresitances with the relation $MR=MR_d+MR_i$, the temperature dependences of the spin polarizations, P, were determined in both Sr_2FeMoO_6 samples as well as in others pseudo-quaternary perovskites – Fig. 5. The spin polarization of sample S-3 is of 58 %, at T = 10 K, and decreases nearly linearly with temperature. The extrapolated temperatures where P= 0, are close to the Curie points. The spin polarization of perovskite S-5, at T = 10 K is nearly half as compared with that evidenced in sample S -3.

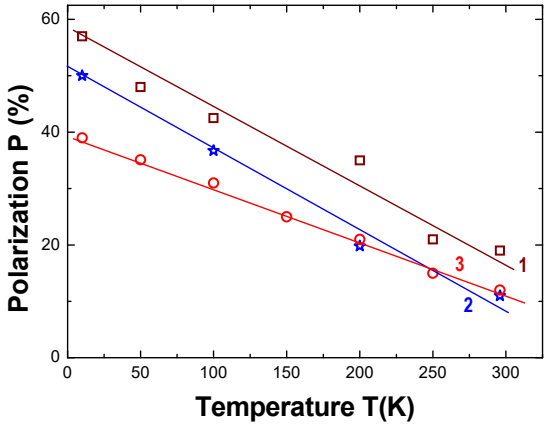

Figure 5. Thermal variations of spin polarizations in 1-Sr_2FeMoO_6 (S-3), 2-$Sr_2FeMo_{0.7}W_{0.3}O_6$, 3- Ca_2FeMoO_6 perovskites.

The comparative analysis of the physical properties of Sr_2FeMoO_6 perovskites sintered in different conditions show: (1) the microstructure of the perovskites, the homogeneity of the grain and at the grain boundary are significantly influenced by the sintering conditions; (2) the magnetic properties are mainly determined by the iron valence states and the antisite content; (3) the transport properties are influenced by the energy of the barriers at the grain boundaries, respectively.

The effect of substitutions of Mo by W [11, 23-25], of Fe by Ni and of Ca_2 by $Ca_{1.5}La_{0.5}$ [13-16] on the physical properties of double perovskites were also analysed. The composition dependences of the Curie temperatures for $A_2Fe_{1-x}Ni_xMoO_6$ with A = Sr and Ca, $Sr_2FeMo_{1-x}W_xO_6$ and $Ca_{1.5}La_{0.5}FeMo_{1-x}W_xO_6$ double perovskites are shown in Fig. 6. Although the Curie points of $Sr_2FeMo_{1-x}W_xO_6$ decrease, as molybdenum is replaced by tungsten, these remain located above the room temperature. The presence of W improve the crystallographic ordering. The increase of sintering time at 1300 °C, from 4 to 8 hrs, leads to a better homogeneity of the grains and diminishes the number of antisites [11]. The cluster glass contribution to the magnetization also decreases. The presence of tungsten, influence only little the magnetoresistance. Even if 30 % of Mo is replaced by W, only a small reduction of spin polarization, as compared to that of the end series member can be shown – Figs. 4 and 5.

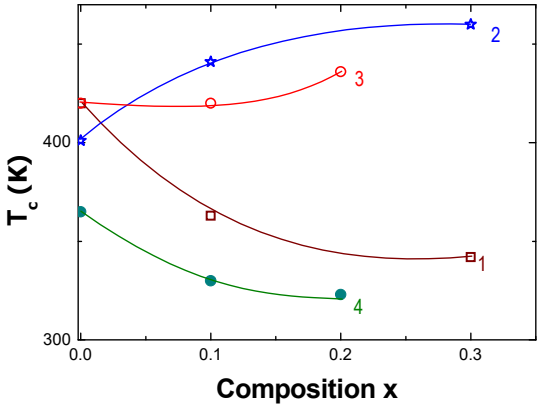

Figure 6. The composition dependences of the Curie temperatures in 1-$Sr_2FeMo_{1-x}W_xO_6$, 2-$Ca_{1.5}La_{0.5}FeMo_{1-x}W_xO_6$, 3-$Sr_2Fe_{1-x}Ni_xMoO_6$ and 4-$Ca_2Fe_{1-x}Ni_xMoO$ double perovskites.

The partial substitutions of Mo by W in $Ca_{1.5}La_{0.5}FeMo_{1-x}W_xO_6$ series, increase also the crystallographic ordering. As a result, higher Curie temperatures and saturation magnetizations, as compared to end series

perovskite, are shown [13]. There are little changes in the magnetoresistances of the W substituted samples. The spin polarization at T = 10 K, increase from 40 % for x=0 up to 53 % when 30 % Mo is replaced by W.

The iron valence states in $Ca_{1.5}La_{0.5}FeMoO_6$ are dependent on pressure. As the pressure increases, the resistivities decrease followed by an abrupt drop at p ≅ 2 GPa [26-28], correlated with changes in iron valence states [26]. This suggests that the transport properties of the perovskites can be tuned by pressure.

The Curie temperatures of $A_2Fe_{1-x}Ni_xMoO_6$ double perovskites increase as iron is substituted by nickel when A = Sr and decrease if A = Ca. The above trend can be analysed in correlation with exchange interactions between B and B' sites magnetizations, resulting from the composition dependence of the antisite content [16].

We note that in $La_{1-x}Pb_xMnO_3$ perovskite, a spin polarization of ≅ 90 % was obtained for a composition x = 0.4 [29, 30]. Unfortunately, the Curie temperatures of the series are rather low and consequently cannot be used in spintronic applications, working at room temperature.

CONCLUSIONS

The physical properties of A_2FeMoO_6 double perovskites with A = Sr, Ca, as well as of series obtained by substitutions at A, Fe and Mo sites are strongly dependent on the sintering process (temperature, time, atmosphere). The partial substitution of Mo by W improve the crystallographic ordering. Their magnetic and transport properties are influenced by aging or by keeping in air.

EXPERIMENTAL SECTION

The double perovskites were prepared by solid state reaction. The amounts of $SrCO_3$, $CaCO_3$, Fe_2O_3, La_2O_3, WO_3 and NiO powders, corresponding to the requested sample compositions, were mixed and calcinated in argon atmosphere at T = 900 ^oC. The calcinated powders were pelletized and sintered at temperatures 1200–1300 ^oC, between 4 and 8 hrs, in a stream of argon flow atmosphere having 0.8 % up to 1.7 % hydrogen.

The XRD spectra showed the presence of only one phase. The spectra were analysed by Rietveld method by using a TOPAS program [31]. In this way, the lattice parameters and antisite (AS) content were determined. The $Sr_2FeMo_{1-x}W_xO_6$ and $Ca_{1.5}La_{0.5}FeMo_{1-x}W_xO_6$ series with x≤0.3, crystallize in

a tetragonal and monoclinic structure types, respectively. The $A_2Fe_{1-x}Ni_xMoO_6$ with A = Sr, Ca perovskites form solid solutions up to x = 0.2.

Scanning electron microscopy (SEM) and energy disperse spectroscopy (EDS) measurements were made with a JEOL-type equipment. The compositions, grain dimensions and the distribution of constituting elements along the grains were analysed.

Magnetic measurements have been performed by extraction method, in the temperature range 4.2 K to Curie points, in fields up to 7 T. The ^{57}Fe Mössbauer studies have been made, at T = 77 K, on Sr_2FeMoO_6 perovskites synthesized in different conditions.

The resistivity and magnetoresistance were investigated in the 10 K ≤ T ≤ 300 K temperature range and fields up to 7 T, by using the four terminal method.

ACKNOWLEDGMENTS

We would like to acknowledge support from the Romanian UEFISCDI project number PN-III-P4-ID-PCCF-2016-0112 Nr. 6.

REFERENCES

1. K. I. Kobayashi; T. Kimura; H. Sawada; K. Terakura; Y. Tokura; *Nature*, **1998**, 395, 677
2. D. Rubi; I. Nogues; J. S. Munoz; J. Fountcuberta; *Mat. Sci. Eng.* ***2006****, B126, 279*
3. R. P. Borges; R. M. Thomas; C. Cullinan; J. M. D. Coey; B. Suryanarayanan, L. Ben-Dor; I. Pinsard-Gaudart; A. Recolevschi; *J. Phys.: Condens. Matter*, **1999,** 11, 1445
4. E. Burzo; Perovskites, *Landolt-Börnstein Handbook, Springer Verlag,* **1996**, vol. 27F1ß
5. K. Kuepper et all; *Phys. Stat. Solidi (a),* **2004**, 201, 3252
6. M. Raekers et all; *J. Opt. Adv. Mater,* **2006**, 8, 455
7. J. M. Greneche; M. Venkatesan; R. Suryanarayanan; J. M. D. Coey; *Phys. Rev.* **2001*,*** B63, 174403
8. D. Yang; T. Yang; Q. Sun; Y. Chen; G. L. Lapronti; J. Alloys. Comp. 728, 337 (2017)
9. J. Navarro; C. Frontera; D. Rubi; N. Mestres; J. Frontcuberta; *Mater. Res. Bull.,* **2003**, 38, 1477
10. K. Kuepper; M. Raekers; C. Taubitz; H. Hesse; M. Neumann; A. T. Young, C. Piamonteze; F. Bondino; K. C. Prince; *J. Appl. Phys.,* **2008**, 104, 036103
11. E. Burzo; I. Balasz; M. Valeanu; I. G. Pop; *J. Alloys Comp.,* **2011**, 509, 105
12. E. Burzo; I. Balasz; S. Constantnescu; I. G. Deac; *J. Magn. Magn. Mater.*, **2007**, 316, e741

13. E. Burzo; I. Balasz; M. Valeanu; D. P. Kozlenko; A. V. Rutkauscas; B. N. Savenko; *J. Alloys Comp.*, **2015**, 621, 71
14. E. Burzo; I. Balasz, *Rom.J. Phys.*, **2017**, 62, 601;
15. E. Burzo; I. Balasz; *AIP Conf. Proc.,* **2016**, 1722, 080003
16. E. Burzo; G. Souca; *J. Mater. Sci.: Mater. Electron.* **2021**, 32, 2200
17. D. Sanchez; J. A. Alonso; M. Garcia-Hernandez; M. J. Martinez-Lope; J. L. Martinez; A. Mellergard; *Phys. Rev.,* **2000**, B65, 104426
18. J. Tejada; B. Martinez; A. Labarta; E. M. Chudnovsky; *Phys. Rev.* , **1991**, B44, 7698
19. Y. Tomioka; T. Okuda; Y. Okamoto; R. Kumai; K. I. Kobayashi; Y. Tokura; *Phys. Rev.* , **2000**, B61, 422
20. G. Suchaneck; N. Kalanda; E. Artiukh; M. Yarmolich; N. A. Sobolev; *J. Alloys Comp.* **2021**, 860, 158526
21. D. Niebieskikwiat; F. Prado; A. Caniero; R. D. Sanchez; *Phys. Rev.,* 2004, B70, 132412
22. D. Serrate; J. M. De Teresa; R. A. Algarabel; M. R. Ibarra; J. Galibert; *Phys. Rev.*, **2005**, B71, 104409
23. S. Ray; A. Kumar; S. Magundar; E. V. Sampathkumaran; D. D. Sarosa; *J. Phys. : Condens Matter,* 13607 (2001)
24. K. I. Kobayashi; T. Okuda; Y. Tomioka; T. Kimura; Y. Tokura; *J. Magn. Magn. Mater.*, **2000**, 218, 17
25. M. Karppinen; H. Yamauchi; Y. Yasukawa; J. Linden; F. S. Chan; R. S. Liu; J. M. Chen; *Chem Mater.,* **2003**, 15, 4118
26. E. Burzo; D. P. Kozlenko; N. T. Dang; S. E. Kichanov; N. O. Golosova; *J. Alloys Comp.*, **2016**, 664, 363
27. P. Zhao; R. C. Yu; F. Y. Li; Z.H. Liu; M. Z. Jin; C. Q. Jin; *J. Appl. Phys.*, **2002**, 92, 1942
28. D. Morrocchelli; P. Postorino; D. D. Castro; E. Arcangeletti; P. Dore; M. C. Guidi; S. Ray; D. D. Sarma; *Phys. Rev.*, **2007**, B76, 172405
29. E. Burzo; I. Balasz; M. Isobe; Y. Ueda, *J. Alloys Comp.***, 2012**, 535, 129
30. E. Burzo; I. Balasz; I. G. Deac; M. Neumann; *Physica,* **2008**, *B*403, 1601
31. *DIFRAC plus TOPAS General profile and structure analysis software for powder diffraction data*, **2001**, Bruker AXS Gmb, Karlsruhe